Electronic Supplementary Material (ESI) for Nanoscale.

Supporting Information

Achieving Ferromagnetic Insulating Properties in $La_{0.9}Ba_{0.1}MnO_3$ Thin Films through Nanoengineering

Chao Yun[a], Eun-Mi Choi[a], Weiwei Li[a], Xing Sun[b], Tuhin Maity[a], Rui Wu[a], Jie Jian[b], Sichuang Xue[b], Seungho Cho[a], Haiyan Wang[b], and Judith L. MacManus-Driscoll[a]*

S1. Difference in the electronic band structure between plain film and nanocomposite

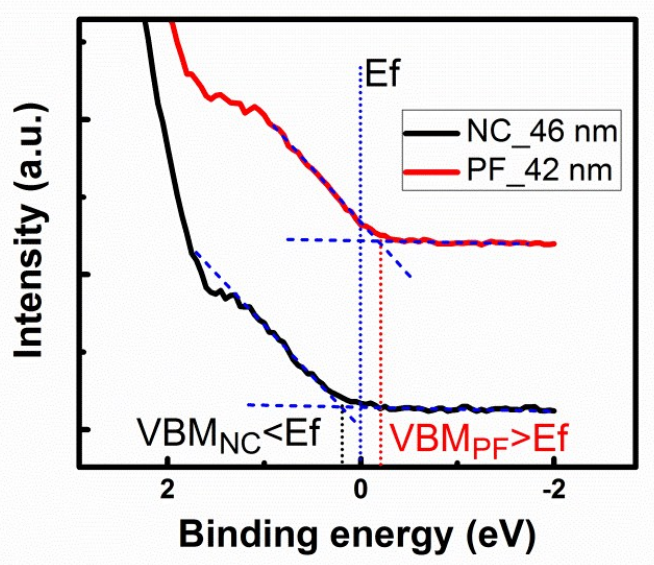

Figure S1. XPS valence band spectra near the Fermi Level for the 42-nm-thick LBMO plain film (PF) and the 46-nm-thick LBMO plain film (PF).

S2. Comparison of ferromagnetic hysteresis loops

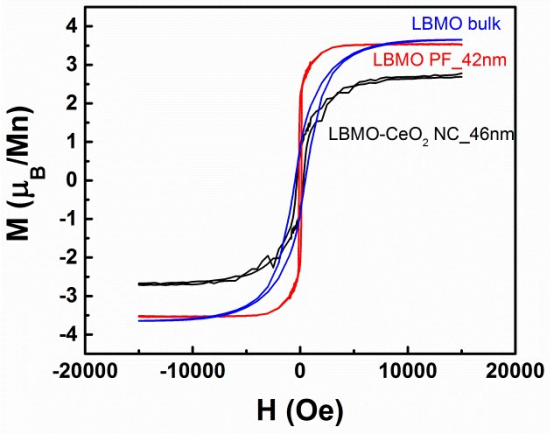

Figure S2. *M-H* curves for the 42-nm LBMO PF, 46-nm LBMO-CeO_2 NC and the LBMO bulk measured at 5 K.

S3. Proof of La-Ce cross-substitution

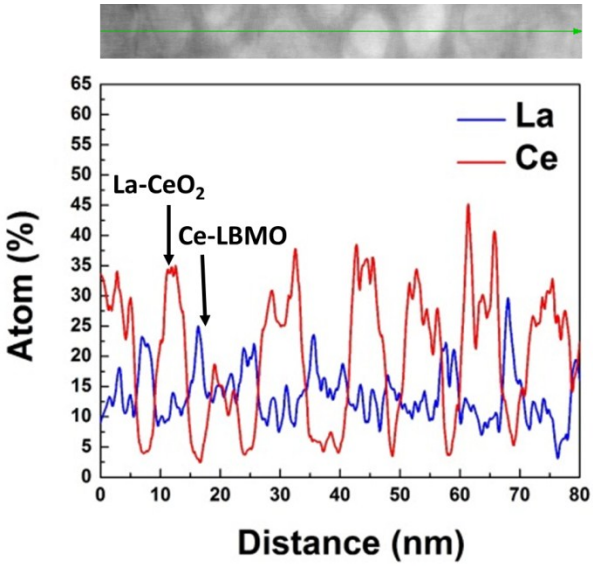

Figure S3. Plan view EDS line profile for the La and Ce elements in the 46-nm LBMO-CeO_2 nanocomposite (NC) film.

S4. Evidence of Ce doping on reducing the double exchange coupling

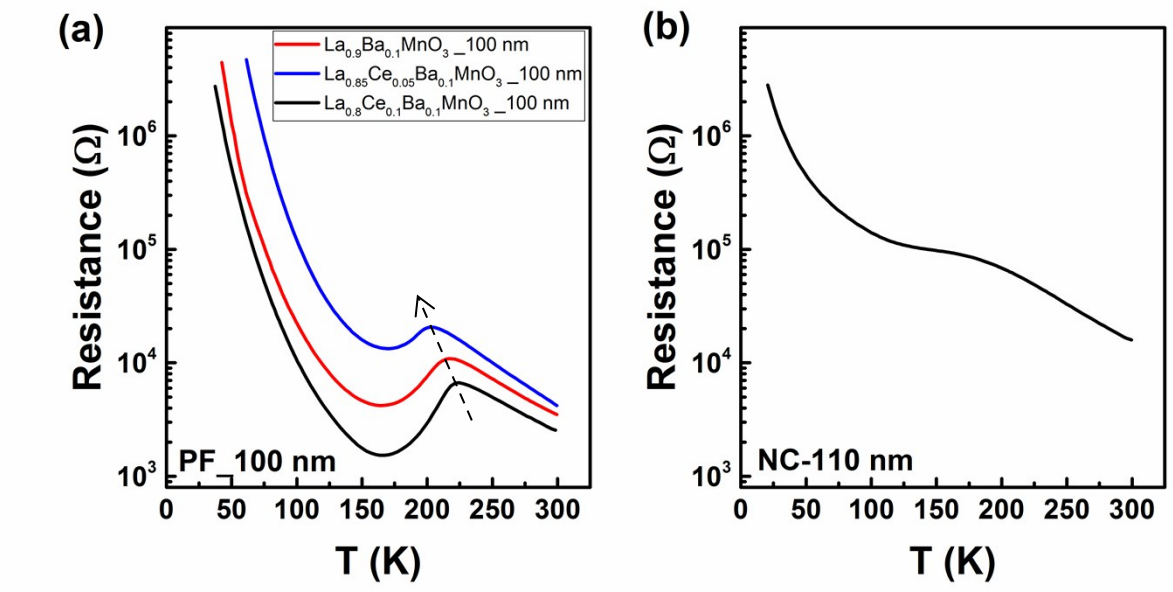

Figure S4. (a) Influence of Ce doping on the transport property of the $La_{0.9-x}Ce_xBa_{0.1}MnO_3$ (x=0, 0.05 and 0.1) plain films (PFs) with a thickness of 100 nm. (b) R-T curve of a 110 nm LBMO-CeO_2 NC.

S5. The influence of Ce doping on double exchange coupling: Defect equations

To understand the conduction behaviour in the bulk, we first consider the defect chemistry of the parent film, $La_{1-x}Ba_xMnO_3$. Ba^{2+} on the La^{3+} site donates holes which are compensated for by the generation of Mn^{4+}. The formation of Mn^{3+}/Mn^{4+} pairs is the origin of the DE coupling, and ferromagnetism/conduction in manganites:

$La_{La}^{x} + BaO = Ba_{La}^{'} + h^{\bullet} + \frac{1}{2}O_2$ (1)

$Mn_{Mn}^{x} + h^{\bullet} = Mn_{Mn}^{\bullet}$ (2)

where La_{La}^{x} represents a La^{3+} ion on a La site, and Mn_{Mn}^{x} and $Mn_{Mn}^{\bullet}$ represent Mn^{3+} and Mn^{4+} on the Mn site, respectively. Hence, for every Ba ion doped on the La site in LBMO, one Mn^{4+} ion is created.

For low Ba doping levels as we have here (x=0.1), a weak level of double exchange (DE) is induced which competes with superexchange (SE) interactions, resulting in an overall FMI[1]. For manganite *films*, on the other hand, cation (both La and alkaline earth) vacancies are prevalent[2] and form thermodynamically under oxidation conditions. Hence, under the growth conditions, cation-deficient LBMO is more stable than the stoichiometric LBMO. This tendency for cation vacancies is higher when the doping level is lower[2,3]. It is believed that the lightly-doped LBMO grown in our growth condition has a tendency to be over-oxidized, leading to cation non-stoichiometry. Therefore, the chemical formula of the films can be written as $La(Ba)_{1-x}Mn_{1-x'}O_3$[7] where x (and x') standard for the non-stoichiometry of the cations. With this in mind, the cation non-stoichiometry of NC and PF can be compared and thus the level of double exchange also compared.

If we consider the formation of La vacancies only, holes are produced which increase the Mn^{4+}/Mn^{3+} ratio, leading to an enhanced DE coupling. Hence,

$La_{La}^{x} + \frac{3}{2}O_2 = V_{La}^{'''} + \frac{1}{2}La_2O_3 + 3h^{\bullet}$ (3)

$3Mn_{Mn}^{x} + 3h^{\bullet} = 3Mn_{Mn}^{\bullet}$ (4)

where $V_{La}^{'''}$ represents a La vacancy on a La site.

In the NC films, when La vacancies pre-exist, Ce^{3+} or Ce^{4+} doping of the La vacancies occurs as a consequence of chemical equilibrium. Two possibilities exist:

(a) Ce exists as Ce^{3+}, and then 3 electrons are generated by filling the La^{3+} vacancies, and these electrons are then compensated by reduction of the Mn^{4+} to Mn^{3+}:

$V_{La}^{'''} + \frac{1}{2}Ce_2O_3 = Ce_{La}^{x} + \frac{3}{2}O_2 + 3e^{'}$ (5)

$3Mn_{Mn}^{\bullet} + 3e^{'} = 3Mn_{Mn}^{x}$ (6)

The reduction of the Mn^{4+} concentration will reduce the DE coupling.

(b) Ce exists as Ce^{4+}, and then 4 electrons are generated by filling the La vacancies. Again, the electrons are compensated by the reduction of Mn^{4+} to Mn^{3+}. Even more Mn^{4+} is reduced compared to the case of Ce^{3+}, and then the DE is further weakened.

$$V_{La}^{'''} + CeO_2 = Ce_{La}^{\bullet} + O_2 + 4e' \quad (7)$$

$$4Mn_{Mn}^{\bullet} + 4e' = 4Mn_{Mn}^{x} \quad (8)$$

S6. Structural information of two thick films

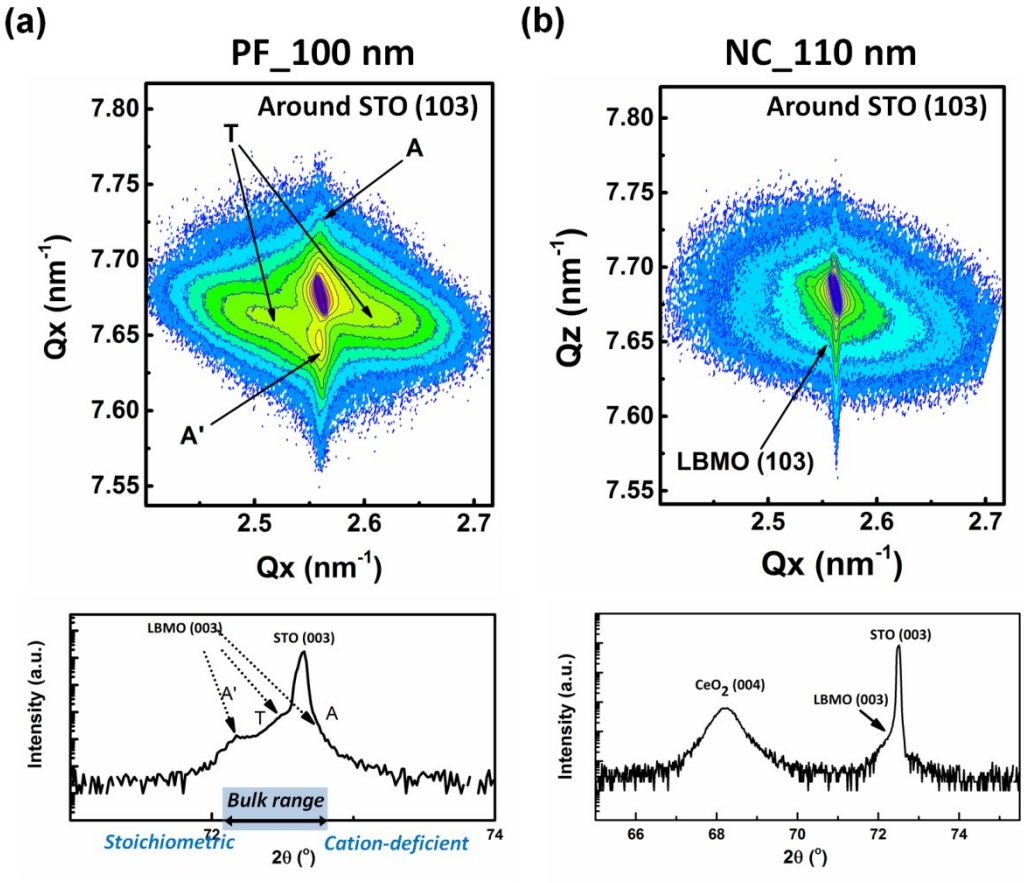

Figure S5. RSM around STO (103) and XRD *2ϑ–ω* scans around STO (003) of (a) 100 nm PF and (b) 110 nm NC.

S7. Structural analysis on the 100-nm LBMO plain film using TEM

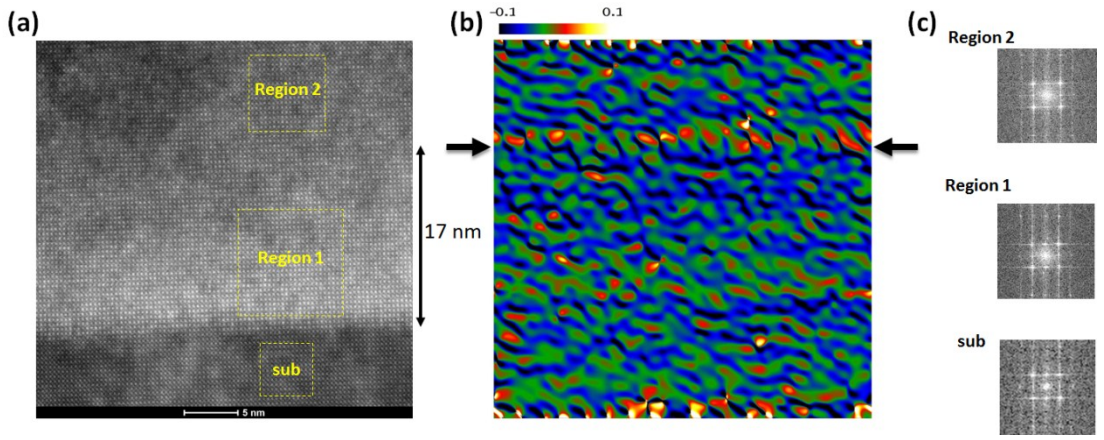

Figure S6. (a) High resolution STEM image of the LBMO PF of 100 nm thickness. (b) The Geometric Phase Analysis (GPA) of out-of-plane strain mapping of ε_{yy} on the image in (a). (c) Fast Fourier Transformation (FFT) of three areas selected in the STEM image in (a): substrate, film area near the substrate and film area away from the substrate.

(1) Local changes in lattice constant. HR-STEM (Fig. S5a) and the corresponding geometric phase analysis (GPA, in Fig. S5b) clearly indicate that there is a transition region (marked by the black arrows in the GPA mapping in (b)) in the film/substrate interface area which is about 17 nm away from the interface. Here 0% strain is referenced to the lattice constant of STO substrate (3.905 Å). The transition region shows obvious red contrast indicating a larger out-of-plane lattice constant in this region. Film Region 1 near to the substrate (first 17 nm) shows more green+blue contrast indicating a small out-of-plane lattice constant. On the other hand, film Region 2 shows more green+red contrast, indicating a higher out-of-plane lattice constant. Hence, there is more in-plane strain in the film in Region 1, as would be expected closer to the substrate interface.

The corresponding Fast Fourier Transformation (FFT) patterns from Regions 1 and 2 and the substrate are shown in (c). They show the epitaxial relation to be cube-on-cube because of good lattice matching (~0.5%) between the film (3.88~3.925 Å) and the substrate (3.905 Å).

(2) Additional proof of the twinning phase. The selected area electron diffraction (SAED) pattern shows obvious diffraction spot splitting in the (00L) direction (Fig. S6a), which is consistent with twin formation. This is confirmed by the peak splitting observed near STO (103) in the RSM, as shown in Fig. S6b. The calculated splitting angle β' of LBMO (103) from the RSM using the model illustrated in Fig. S6b is around 0.25 degree, which is an indication of the periodic tilt angle of twinning. This is in broad agreement with the fact that the measured angle, β, from the LBMO (00L) peak in SAED is very small, <1 degree. This small tilt angle makes it hard to observe twinning in HRTEM images. We note that similar results have been reported in lightly doped $La_{0.9}Sr_{0.1}MnO_3$ (orthorhombic in bulk, and having a small lattice mismatch with STO, which is similar to $La_{0.9}Ba_{0.1}MnO_3$) where the ED spot splitting and RSM paired peak were suggested to originate from coherent twinning[4-6].

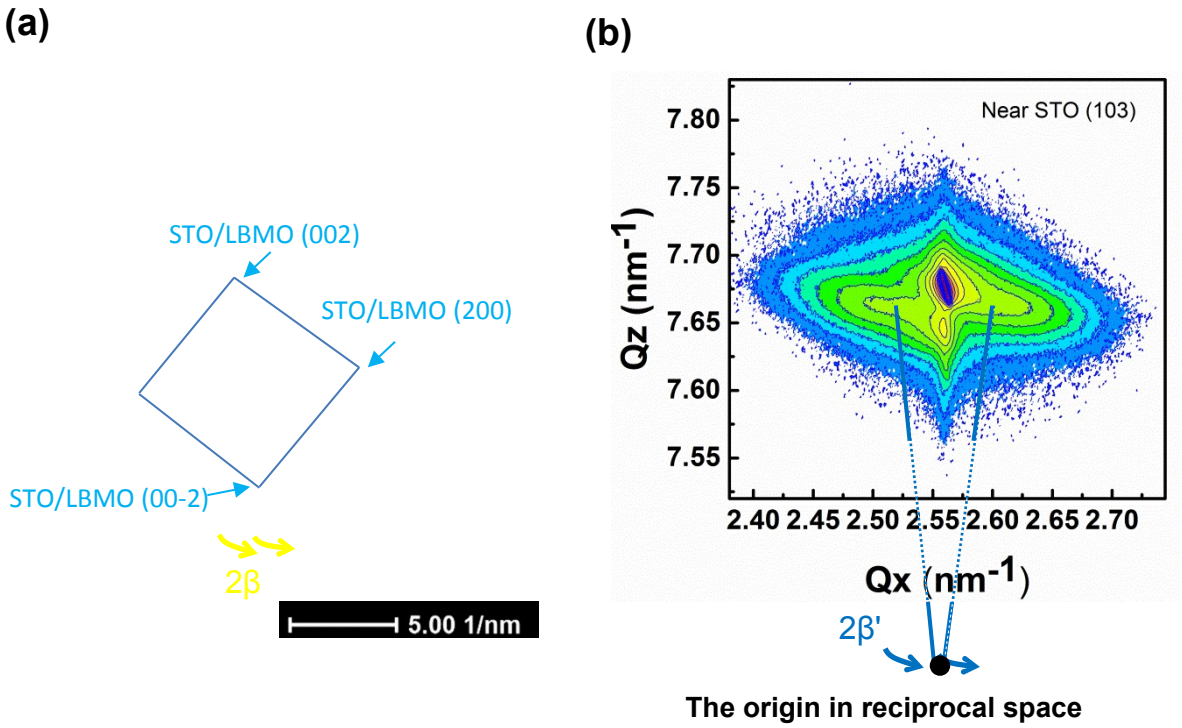

Figure S7. (a) Selected Area Electron Diffraction (SAED) pattern of the 100-nm LBMO plain film. (b) Reciprocal Space Map (RSM) around STO (103) of the same film. The angles β and β' obtained from the spot splitting in the SAED pattern and peak splitting of RSM are an indication of the twinning angle. For simplicity, the dotted line is used to show the angle β' in (b), while the real origin position should be further away.

References

(1) Yi, H.; Yu, J. Double-Exchange Model with Background Superexchange Interactions: Phase Diagrams of $La_{1-x}A_xMnO_3$ Manganites. *Phys. Rev. B* **1998**, *58* (17), 11123–11126.

(2) Mizusaki, J.; Mori, N.; Takai, H.; Yonemura, Y.; Minamiue, H.; Tagawa, H.; Dokiya, M.; Inaba, H.; Naraya, K.; Sasamoto, T.; et al. Oxygen Nonstoichiometry and Defect Equilibrium in the Perovskite-Type Oxides $La_{1-x}Sr_xMnO_{3+d}$. *Solid State Ionics* **2000**, *129* (1), 163–177

(3) Murugavel, P.; Lee, J. H.; Yoon, J. G.; Noh, T. W.; Chung, J. S.; Heu, M.; Yoon, S. Origin of Metal-Insulator Transition Temperature Enhancement in Underdoped Lanthanum Manganite Films. *Appl. Phys. Lett.* **2003**, *82* (12), 1908–1910.

(4) Lebedev, O. I.; Van Tendeloo, G.; Amelinckx, S.; Razavi, F.; Habermeier, H.-U. Periodic Microtwinning as a Possible Mechanism for the Accommodation of the Epitaxial Film-Substrate Mismatch in the $La_{1-x}Sr_xMnO_3$ /$SrTiO_3$ System. *Philos. Mag. A* **2001**, *81* (4), 797–824.

(5) Razavi, F. S.; Gross, G.; Habermeier, H.-U.; Lebedev, O.; Amelinckx, S.; Van Tendeloo, G.; Vigliante, A. Epitaxial Strain Induced Metal Insulator Transition in $La_{0.9}Sr_{0.1}MnO_3$ and $La_{0.88}Sr_{0.1}MnO_3$ Thin Films. *Appl. Phys. Lett.* **2000**, *76* (2), 155–157.

(6) Santiso, J.; Balcells, L.; Konstantinovic, Z.; Roqueta, J.; Ferrer, P.; Pomar, A.; Martínez, B.; Sandiumenge, F. Thickness Evolution of the Twin Structure and Shear Strain in LSMO Films. *CrystEngComm* **2013**, *15* (19), 3908.